Chem Rev Lett 7 (2024) 773-785

Research Article

Chemical Review and Letters
journal homepage: www.chemrevlett.com
ISSN (online): 2645-4947 (print) 2676-7279

Micellar properties and partial phase diagram of cetyltrimethylammonium bromide and cetylpyridinium chloride in vicinity of Krafft point from conductometry and dynamic light scattering measurements

Rachida Aribi[1], Cherifa.Zelmat[1,2], Teffaha Fergoug[1], Youcef Bouhadda[1,*], Meriem Dadouch[1,3], Fatima Yssaad[1], Aicha Kadiri[1] and Fatima Zohra Chater[1]

[1]*Laboratory of Physical Chemistry of Macromolecules and Biological Interfaces, University of Mascara, Mascara 29000, Algeria*
[2]*Departement of chemistry, University Djillali Liabes of Sidi Bel Abbes, Sidi Bel Abbes 22000, Algeria*
[3]*Departement of pharmacy, Faculty of Medicine, University Djillali Liabes of Sidi Bel Abbes, Sidi Bel Abbes 22000, Algeria*

ARTICLE INFO

Article history:
Received 24 June 2024
Received in revised form 12 September 2024
Accepted 17 September 2024
Available online 20 September 2024

Keywords:
Conductivity
Surfactant
Dynamic light scattering
Krafft point
Phase diagram
thermodynamic parameters

ABSTRACT

Solubility and micelle formation of cetyltrimethylammonium bromide CTAB and cetylpyridinium chloride CPC surfactants in aqueous solution have been studied by tensiometry, conductometry, and dynamic light scattering (DLS) in the vicinity of Krafft point. Parameters such as the critical micelle concentration (cmc), Krafft temperature (Tk), average micelle aggregation number (n) and phase diagram of surfactants in water were determined and thermodynamic micellization process was discussed in light of enthalpy and entropy contributions. It is shown that unlike CTAB surfactants which exhibit incubation time independent micellar behavior, CPC surfactants show two solubility curves in the vicinity of Krafft temperature leading to complex temperature conductivity concentration plots. The change of solubility and cmc with temperature were investigated according to the mass action thermodynamic model and permit to extract free energies of micelles formation and to draw partial phase diagram for each surfactant. Dynamic light scattering techniques shows that according to the incubation conditions, different population of micelles can be released in the vicinity of Krafft temperature.

1. Introduction

Surfactants are widely used in industries and medical preparations. They are by all means surface-active, able to adsorb to air-water surfaces and/or oil-water interfaces. This is due to their dual property nature, containing a hydrophobic chain at one end and a hydrophilic head at the other one[1**,** 2]. When dissolved in aqueous solutions, surfactant molecules self-assemble to form micelles to minimize the water-oil contact and this occurs when surfactant concentration exceeds a critical concentration known as the critical micelle concentration (*cmc*) [3,4]. This interface/surface adsorption ability explains the dissolution of organic matter into aqueous media and the transformation of hydrophilic solid surfaces to hydrophobic ones and reciprocally. *cmc* is highly dependent on many thermodynamic parameters such as temperature and pressure as well as solution ionic strength, surfactant polar head nature and its counter ion, etc...

It is known that for ionic surfactants above the *cmc* the solubility would experience a rapid increase when the temperature reaches the Krafft temperature (T_k), which corresponds to the temperature where the insoluble surfactant hydrated crystals start to melt and contribute to the bulk solution as micelles or free surfactant molecules. The temperature corresponding to the melting of the last hydrated crystal is referred to as the melting temperature (T_m), which is concentration-dependent. These two specific temperatures are well distinguished in mass action thermodynamic model but in phase separation one

* Corresponding author.; e-mail: y.bouhadda@univ-mascara.dz
https://doi.org/10.22034/crl.2024.464501.1363

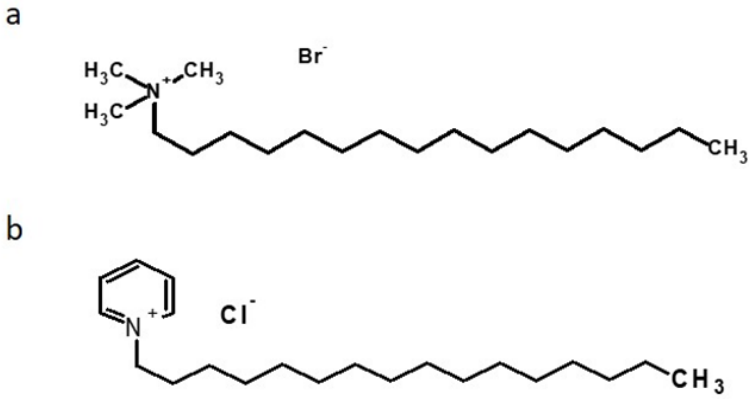

Fig. 1. Chemical structure of (a) cetyltrimethylammonium bromide (CTAB), (b) cetylpyridinium chloride (CPC).

only (T_m) is recognized as Krafft point. According to the method described by Gaboriaud *et al*. [5] depending on the concentration, surfactant thermal dissolution typically shows three sections that characterize the successive dissolution balances. The first one below Krafft temperature corresponds to a saturated solution that contains only monomer species in equilibrium with suspended surfactant hydrated crystals. The second one which is distinguished by a significant rise in solubility along a concentration-dependent variable temperature range corresponds to the mutual balances gathering micelles, free surfactants, and surfactant hydrated crystals. The lower temperature in this section corresponds to (T_k) whereas the superior limit corresponds to (T_m), hence the corresponding concentration at (T_m) designates the total solubility. Beyond (T_m) (third section) the micelles are in equilibrium with the free surfactants beyond the *cmc*. The Gaboriaud method [5] permits extraction from the conductivity-temperature and conductivity-concentration curves the total solubility curve of the surfactant in terms of micelles and monomers in the vicinity of the Krafft and melting temperatures. This method was successfully applied to SDS as a model surfactant and to other surface active compounds as tetracaine [6] and 1-heptodecafluorodecyl-pyridinium Iodide (HFDPyI) [7].

In this work, we explore the solubility curves of two cationic surfactants which contain in their respective polar head group a nitrogen atom with different configurations, in the vicinity of their corresponding Krafft point. The first molecule is the cetyltrimethylammonium bromide surfactant (CTAB) which possesses a tetrahedral ammonium atom and the second one is the cetylpyridinium chloride surfactant (CPC) which contains a planar ammonium atom in the pyridinium polar head (Figure 1). This latter surfactant is found in many applications as a corrosion inhibitor of steel [8-11] and as a biocidal agent against a wide range of microorganisms, including *Staphylococcus aureus* [12-14]. During the SARS-CoV-2 pandemic, clinical trials for CPC were conducted to determine how it would affect morbidity since it was thought that its structure interacts with the virus membrane [15-17]. Many fundamental studies have also been carried out on CPC, mostly to determine the transport parameters of CPC monomers [18], the *cmc* and Krafft transition points [19, 20]. In this context, several studies [20-22] reported (T_k) values around 10°C whereas other authors [23-25] found values from 15°C to 20°C. This disparity in values is not only ascribable to the variability in the used techniques but is also the fruit of dynamics effects accompanying the (T_k) transition as proposed later by Sasaki and al. [19, 20,26] in a series of research papers**.** They found from small-angle X-ray scattering (SAXS), electrical conductance and calorimetry measurements that CPC exhibits two hydrated crystal phases in the Krafft region. They showed that depending on the incubated time lasted prior to the warming experiments one of the two phases designed as the metastable form melts earlier compared to the most stable one which can reach melting temperatures beyond 20°C. One of the interesting issues addressed in these works was the establishment of the phase transition boundary curves and the kinetics of such phenomenon.

In the present study, the micellar behavior of (CPC) and (CTAB) surfactants is investigated in the vicinity of their corresponding Krafft point using dynamic light scattering (DLS) at different temperatures and incubation times. The severalty of T_k and T_m values for (CPC) surfactants reported in literature will be solved in the light of the (DLS) and conductivity studies undertaken herein. It will be shown that the combination of (DLS) and conductivity measurements can lead to an accurate description of the micellar systems usually acquired by time consuming and expensive techniques such as (SAXS) and (ITC) [19, 20,26]. An appropriate

thermodynamic description based on the classical mass action model (MA) will be undertaken which will permits thermal analysis to determine parameters such as *cmc*, (T_k), (T_m), average micelle aggregation number (n) and the change of solubility with temperature. The severalty of T_k and T_m values reported in literature will be solved in the light of the physical chemistry studies undertaken herein. From *cmc* data, the free energies of micelles formation were calculated and enthalpy and entropy contributions to the micellization process were discussed.

2. Materials and methods

2.1. Reagents

The cetyltrimethylammonium bromide CTAB and cetylpyridinium chloride CPC surfactants with a purity of 99 % supplied by Sigma were used without further purification. All the solutions were prepared with purified water (taken from a Genpure Millipore Super-Q System), with conductivity lower than 2.06 µS/cm.

2.2. Solution preparation

The aqueous stock solution of each surfactant was first prepared at room temperature, warmed enough until complete dissolution of the solid, and finally cooled to 276 K (3°C) to induce crystallization. Once the system is in equilibrium (solution stands for 1 hour), it is heated in steps of 0.1 K min^{-1} to ambient temperature. Each sample solution is obtained by the appropriate successive dilutions of the stock solution at ambient temperature. Before each set of measurements, all solutions are allowed to stand for one day. The homogeneity of the initial solutions was assured by sonication for three hours in an ultrasonic bath.

2.3. Specific conductivity

Conductivities were measured using a Knick-type conductimeter with a 4-poles electrode calibrated with NaCl and KCl aqueous solutions. The conductivity range was from 1 µS/cm to 1000 mS/cm with an accuracy of 0.5%. During the conductivity measurement of heterogeneous surfactant suspension, the sample solution was stirred gently and continuously with a magnetic stirrer. To better visualize the variation of the specific conductivity between the different curves, specific conductivities were normalized as $\kappa = \kappa(T) - \kappa(T_0)$ where T_0 being the lowest temperature and T the working one. The *cmc* value was taken at the break in the conductivity vs. concentration plots at different temperatures.

2.4. Surface tension

Surface tension was measured using a Lauda TC1 De Nouiy® tensiometer with a circular platinum-iridium ring of 6 cm. The measured values are reproducible to within ± 0.05 mN/m and it can be obtained by a direct scale reading. The reading on the apparatus gives directly the applied force of the pull exerted on the ring or the apparent surface tension. The measurements were performed, at (298 ± 0.01) K for CTAB and (301 ± 0.01) K for CPC for different concentrations.

2.5. Dynamic light scattering DLS

DLS experiments were performed on a nano-ZS Zetasizer model 3600 (Malvern Instruments, UK) equipped with a He–Ne laser (λ = 633 nm, 4.0 mW) working at an angle of 173° and equipped with a thermostatic sample chamber. The time-dependent correlation function was measured at different temperatures for different concentrations of surfactants above their respective *cmc* in water and was analyzed in cumulative mode using the integrated Zetasizer software. The instrument software (Malvern zetasizer® software v.7.11) provides three different alternatives to quantify size distribution based on intensity, volume and number. All data values are the average of at least three measurements. The studied solutions were prepared according to solution preparation section but were further incubated during different periods as will be specified later in the text.

3. Results and discussion

3.1. Surface tension results

Figure 2 shows the plots of variation of surface tension (γ) against the concentration of CTAB and CPC surfactants in aqueous solutions at T = 25°C (298K) for the former and T = 28°C (301K) for the latter. It is obvious to note that no minimum exists for every curve which underlines the purity of the prepared samples. The decrease in the surface tension accompanying the increase in surfactants concentration for both solutions proves that CPC and CTAB have a noticeable surface activity at the water-air interface which induces solution surface tension to drop until approximately γ_{min} ~ 39 mN/m for CPC and 35 mN/m for CTAB. On each curve, the break point corresponds to the *cmc* which can be determined from the intersection of the linear fitting of the points in the decreasing regime and in the plateau one. For CPC the obtained value of *cmc* was 0.85 mM whereas for CTAB a *cmc* of 1 mM was deduced. These results agree with reported literature data about each surfactant for γ_{min} and

for *cmc* with the same technique [27-29]. Using the Gibbs adsorption isotherm, the surface excess concentration (Γ) can be obtained from the slope of the linear fit of the data below the *cmc*:

$$\Gamma = -1/2RT\partial\gamma/\partial \ln C \quad (1)$$

Afterwards, the minimal area per molecule (A) can be calculated from the equation:

$$A = 1/N\Gamma \quad (2)$$

where N corresponds to the Avogadro's number.

The minimal area per molecule obtained for CTAB is 56.1 Å2 at 25°C which agrees with literature reported data [27, 29]. However, the obtained value for CPC 207 Å2 at 28°C was far from reported ones [30, 31]. The π_{mic} value, defined as the difference between the surface tension of pure water (γw) and that of the solution at the cmc (γcmc), has been deduced and reported in Table 1.

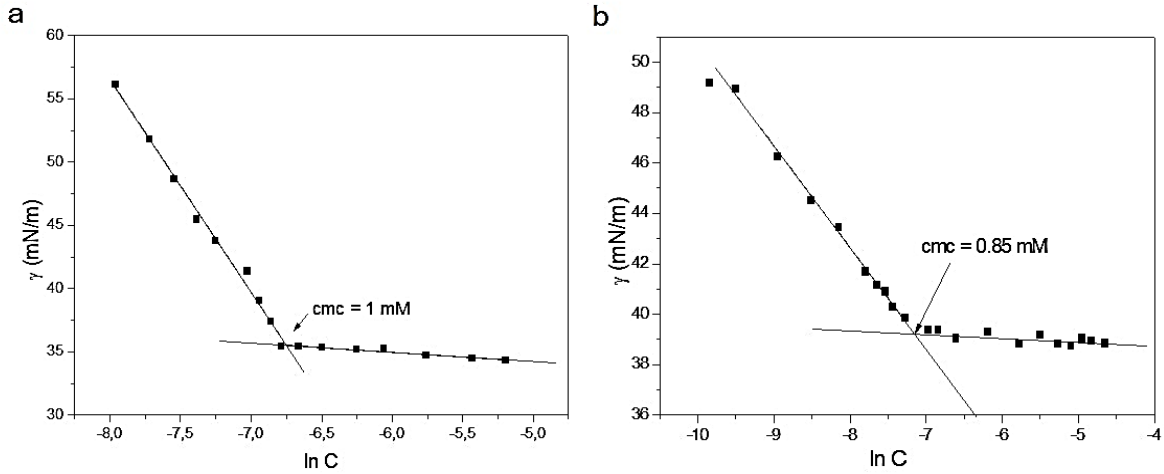

Fig. 2. Variation of the surface tension (γ) of (a) CTAB and (b) CPC solutions vs concentration, at 25°C and 28°C respectively.

Table 1. Interfacial properties of CTAB and CPC in water at 25°C and 28°C respectively by Surface Tension

Samples	T (°C)	*cmc* (mM)	γ_{cmc} (mN/m)	π_{cmc} (mN/m)	$\Gamma.10^6$ (mol/m^2)	a_0 (Å^2)
CTAB	25	1.02	35.2	37.8	2.9	56.1
CPC	28	0.85	39.2	33.8	0.8	207

3.2 Dynamic light scattering

Figure 3 shows the scattered dynamic light intensity variation by size for CPC and CTAB aqueous solutions equilibrated at 30°C for concentrations far above their corresponding *cmc* values. These two size distribution profiles are typical to surfactants solutions, with a weak signal at a size range under 10 nm ascribable to micelle particles and diverse bands or peaks spread along the high size domain (above 100 nm) related to water-surfactant nanostructures [32, 33]. These typical profiles are sensitive to the variation of temperature, surfactant concentration, and the presence of additives in a way that some water nanostructures related signals can be minimized or shifted. Usually, in surfactant studies, an amount of salt is added to the micellar solution to increase the micelle signal and minimize the water-surfactant nanostructures ones.

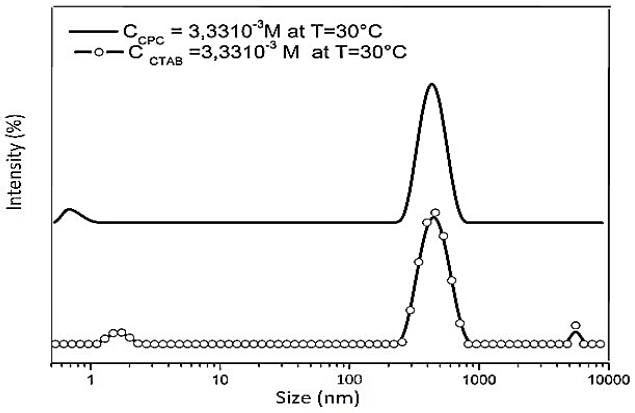

Fig. 3. Scattered light intensity variation by size for CTAB and CPC aqueous solutions equilibrated at 30°C.

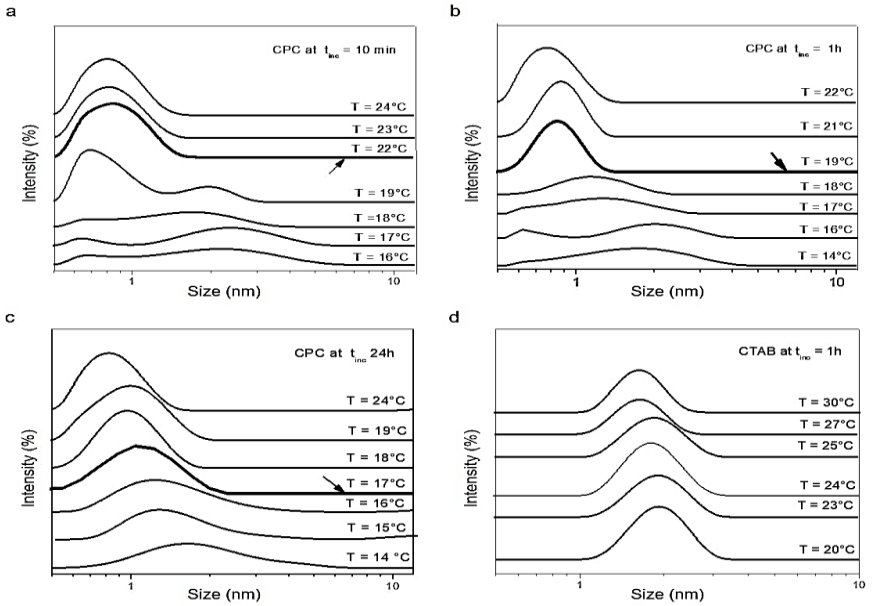

Fig. 4. Scattered light intensity vs size curves for 100 mM aqueous CPC solutions incubated at 5°C for different periods (a) 10 min, (b) 1h, (c) 24h, and of 3,33 mM CTAB solutions incubated at 15°C (d) for 1h.

However, the drawback of the salt addition is an unavoidable shift in micelle size peak position and no insurance of the total disappear of water-surfactant nanostructure signals.

Moreover, from the results (no shown herein) of the variation of scattered light by number and volume against size it was clear that the micelle species constitutes the dominant contributor to the total signal by intensity, thus we have chosen to work with salt free solutions and to ignore the peaks of water-surfactant nanostructure species as long as they don't interfere with micelle signal (overwrite the micelle signal). In this work, for DLS measurements only the temperature effect was investigated in parallel to the effect of incubation time on the micelle size so only the micelle size signals domain were considered.

Figure 4 shows the scattered light intensity variation against size for CPC aqueous solutions at different temperatures for various incubation periods t_{inc} (10 min, 1h, and 24h) at 5°C before measurements during warming and for CTAB solutions at different temperatures for an incubation period of t_{inc} = 1h at 15°C. Firstly, it is remarkable in the case of CPC solutions that the shape and the number of peaks depend on the t_{inc} andthat a particular limit temperatures T_{par} exist beyond which only a single peak is observed (resolved) (T_{par} = 17°C for t_{inc} = 24h, T_{par} = 19°C for t_{inc} = 1h, and T_{par} = 22°C for t_{inc} = 10 min)**.** For CTAB surfactant, whatever the temperature is only one clear peak is obtained and logically corresponds to one CTAB micelles type. For every studied solution of CPC below the corresponding particular temperature, the size distributions suggest the presence of different micellar species differently sensitive to the incubation time of the initial solution. This hypothesis is corroborated by results published by Sasaki *et al.* [19] whom from differential scanning calorimetry measurements on CPC solutions, over temperatures ranging from 5 to 30°C, observed for the CPC solution incubated at 5 °C for a period shorter than 6 h the appearance of two peaks which reduces as a single one when the temperature rises above 19 °C. When the same solution was incubated at 5 °C for a longer period than 6 h, only one single endothermic peak was obtained along the range of studied temperatures. They explained the second peak on the enthalpogram by the existence of a metastable surfactant hydrate crystal that grows faster with temperature increase but melts at a lower melting temperature (12°C) compared to the stable crystalline one. The same results are also corroborated by SAXS and SANS experiments conducted by the same authors where two species were reported for an incubation time of 10 min at 5°C and only one for an incubation period of 24h [19]. For our case from DLS experiments and according to the temperature range investigated (above 12°C), only the micelles derived from the most stable crystalline phase are expected to appear and they seem to size homogenize with increasing temperature until to resolve as a unique-size particles beyond the particular temperature. These observations underline the importance of the incubation time at low temperatures (crystallization) before the beginning of the warming experiments and complete the Sasake team observations which were focused only on the crystal entities. It is clear that as short as the incubation

Table 2. Thermal variation of aqueous CTAB and CPC surfactants solubility for C > *cmc*

CTAB							
C (mM)	250	100	50	10	1.5		
T_m (°C)	33	30	28	27	26		
CPC							
C (mM)	100	66.6	44.4	29.6	19.7	9.85	6.56	4.37
T_m (°C)	24.7	24.6	23.7	23.2	23	21.7	21	20.7

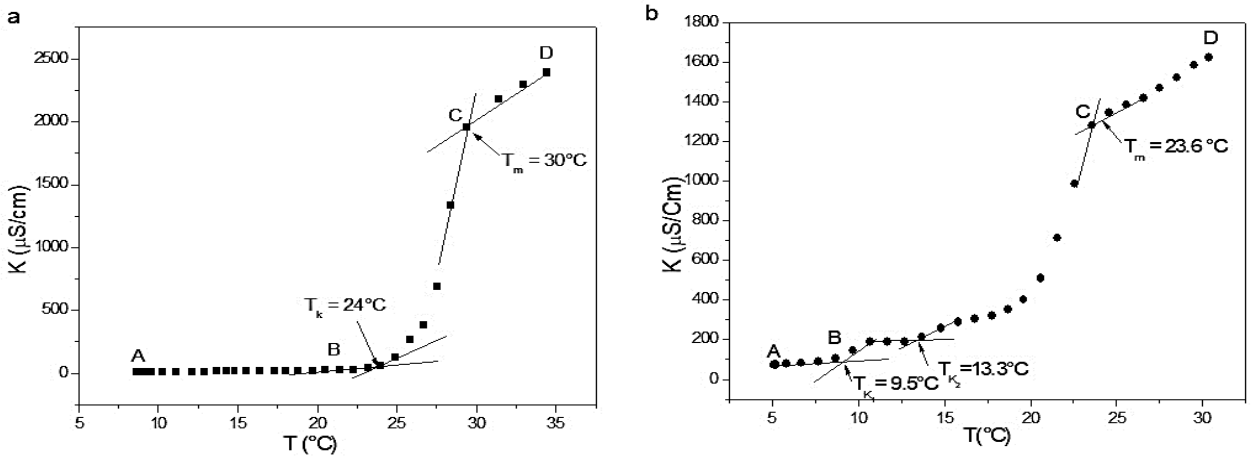

Fig. 5. Evolution of the specific conductivity, $K=K(T)-K(T_0)$ *vs* temperature for (a) CTAB and (b) CPC at C =100 mM and 44.4 mM, respectively and geometric determination of the T_k and T_m points of the CTAB and CPC surfactant in water solution**.**

time is as high as is the micelle size polydispersity and melting temperatures.

3.3. Conductivity results

Effect of temperature

Figure 5 shows the thermal variations of the normalized specific conductivity of CTAB and CPC aqueous solutions at concentrations above their respective *cmc* values. According to the Gaboriaud method described elsewhere [5, 7] and depending on the concentration, conductivity curves show three portions [A-B]; [B-C] and [C-D] which characterize the successive dissolution balances. In figure 5.a that corresponds to 100 mM of CTAB; the portion below Krafft temperature is a saturated solution that only contains monomer species. The [B-C] branch comes
next and is distinguished by a significant rise in conductivity and hence in solubility. The length of the [B-C] domain differs according to the balance between micelle phase and solid one (hydrated crystal) at different concentrations as shown in Figure 6. The lower point B, corresponds to Krafft temperature T_k whereas the superior limit indicated by various C points, correspond to the melting temperatures T_m, therefore the corresponding concentrations designate the total solubility. Beyond T_m (third portion [C-D]) the curve presents a sharp slope change characterized by a lowering of the conductivity increase attributed to the lower mobility of the micelles. It is worth to emphasize that the conductivity curve of CPC surfactant (Figure 5.b) is somewhat different from one reported for CTAB (Figure 5.a) on the [B-C] portion. For CPC surfactant, this portion seems to contain jumps ascribable to the metastable species already mentioned in the DLS measurements analysis herein. So unlike CTAB surfactant which presents a unique T_k, CPC surfactant seems to have several T_k ascribable to at least two metastable species. This CPC feature joins the observations of Sasake *et al*. on CPC surfactant phase transition in the Krafft domain deduced from robust techniques such as DSC, SAXS, and SANS where two hydrated crystals were identified. From the different thermal curves on figure 5, the Krafft temperature value of CTAB is obtained straight forwardly $T_k \approx 24$ °C, a value which is in accordance with literature data [34-36]. For CPC surfactant, different T_k values are reported by different authors undoubtedly due to the difference in used characterization techniques and also to the adopted experimental protocols in terms of incubation time (existence of metastable hydrated crystals). Nevertheless, compared to other surfactants, CPC has low Krafft temperatures, and thus a very weak solubility at temperatures lower than $T_{k_1} \approx 9.5$°C for the metastable hydrated crystal and $T_{k_2} \approx 13.3$°C for the more stable one

as in figure 5.b. The second important information deducible from the curves in figure 6 is the T_m temperature which corresponds to surfactant solubility. Table 2 gathers the values of T_m obtained for every surfactant at different concentrations. For each surfactant, T_m temperature varies according to surfactant concentration, unlike T_k which is distinct with regard to the mass action model.

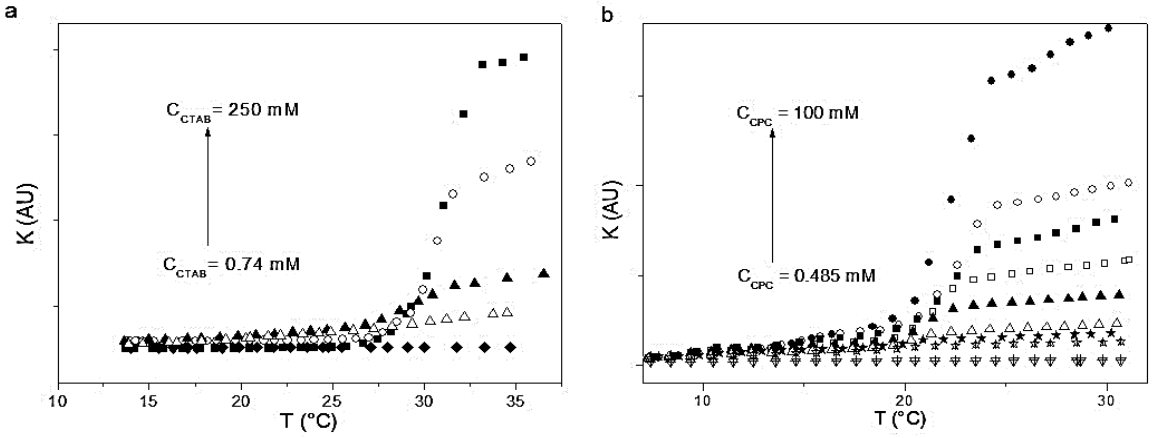

Fig. 6. Evolution of the specific conductivity, $K=K(T)-K(T_0)$, as a function of temperature for different concentrations of the (a) CTAB and (b) CPC surfactants in water solution.

The *cmc* values are straightforwardly determined from conductivity-concentration curves plotted in figure 7. For CTAB surfactant every plot shows two linear regions that cross at the *cmc*. It is also easy to determine the degree of dissociation (α) from the ratio of the slopes above (S_2) and below (S_1) the cross point. The corresponding (α) values and *cmc* values are gathered in table 3. The conductivity-concentration curves of CPC are different with two break points for some curve and only one for others. For temperatures below T = 30°C three linear portions are observed and only two portions are obtained for temperatures above 30°C, similarly to the CTAB case. The intermediary portion for CPC surfactants shrinks when the temperature increases which may indicate the presence of an intermediary micellar phases between the free surfactant phase and final micellar phase (close S2 slope).

According to table 2, for temperatures in the range of 22-23°C, the solubility is around 10 to 20 mM which covers almost the concentration domain scanned in figure 6. This means that the system is set at the boundary of its micellar solubility area and not only (free surfactant, micelle) balance exists but also (free surfactant, solid hydrated crystal) and (micelle, solid hydrated crystal) balances coexist. In these temperature ranges the excess of surfactant contributes more to the formation of the intermediary phase than the formation of more common micelles. The obtained *cmc* values at 25°C and 28°C (see table 3) for CTAB and CPC respectively are slightly different from *cmc* values deduced from tensiometry measurement. Nevertheless, these differences are mainly due to the nature of detection technique where the tensiometry looks at superficial molecules in equilibrium with ones in the bulk while the conductivity deals with exclusively bulk molecules. From the degree of dissociation (α) values, it appears that CTAB surfactant counter-ions are better bounded to their corresponding micelles compared to CPC ones.

3.4. Determination of solubility curve results

According to Moroi *et al.* [37] two contributions control the variation of the total solubility with temperature. The first one, $C_{1,t}$, results from the molecular dissolution of the surfactant, whereas the second one, $C_{2,t}$, represents the dissolution of the surfactant in the monomeric state coexisting with micelles. In order to estimate the solubility below the *cmc*, the conductivity for a given concentration C < *cmc* is compared to a model plot of the conductivity variation with concentration in the region C < *cmc* at the corresponding temperature as illustrated in figure 8.

For every surfactant, the measured results lead to the following equations for the solubility $C_{1,t}$:

$$\mathrm{Log}[C_{1,t}]_{CPC} = 0.013\ T - 3.56 \quad (3)$$

$$\mathrm{Log}[C_{1,t}]_{CTAB} = 0.00654\ T - 3.5 \quad (4)$$

Therefore, given the total solubility, the second contribution to total solubility $C_{2,t}$ can be deduced as:

$$\mathrm{Log}[C_{2,t}]_{CPC} = 0.32\ T - 9.08 \quad (5)$$

$$\mathrm{Log}[C_{2,t}]_{CTAB} = 0.3127\ T - 10.304 \quad (6)$$

Thus, the total concentration at saturation equation is deduced (Eq. (7) and (8)) and their curves are shown in Figure 9.

$C_{t,CPC} = C_{1,t} + C_{2,t} = 10^{[0.013T - 3.56]} + 10^{[0.32\ T - 9.08]}$ (7)

$C_{t,CTAB} = C_{1,t} + C_{2,t} = 10^{[0,00654T - 3,5]} + 10^{[0,3127\ T - 10.304]}$ (8)

From the conductivity behavior of CTAB and CPC, it is obvious that these results match well with the mass action model. The partial phase diagrams of CTAB/water and CPC/water deduced from conductivity measurements are shown in figure 10 for concentrations below 60 mM (CTAB)/14 mM (CPC) and temperature domain ranging from 0 to 40°C. From the conductivity measurements, it is easy to recognize the usual 4 zones delimited by both solubility and *cmc* curves as well as Krafft temperature line. In the zone (I) the molecular non-saturated aqueous solutions separated by the *cmc* curve from zone (II) which corresponds to a limpid macroscopic homogenous micellar phase.

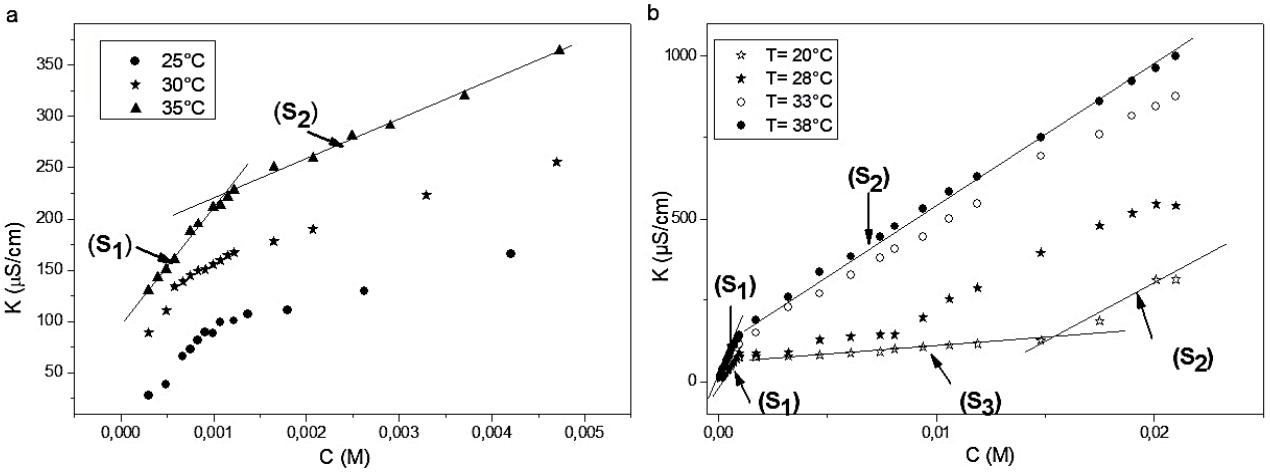

Fig. 7. Variation of the conductivity, κ, *vs* concentration, for (a) CTAB and (b) CPC at different temperatures.

Table 3. *cmc* values and degree of dissociation (α) of CTAB and CPC at different temperatures by conductimetry

CTAB				
T(°C)	25	30	35	/
cmc (mM)	0.97	1.1	1.2	/
α	0.20	0.24	0.35	/
CPC				
T(°C)	28	33	35	38
cmc (mM)	1.03	1.09	1.14	1.16
α	0.35	0.37	0.38	0.40

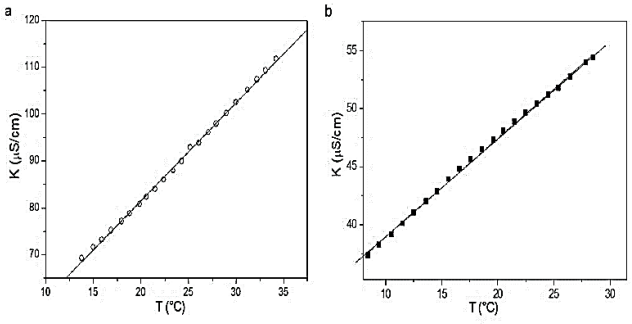

Fig. 8. The conductivity at *C* < *cmc;* (a) CTAB at 0.74 mM and (b) CPC at 0.485 mM.

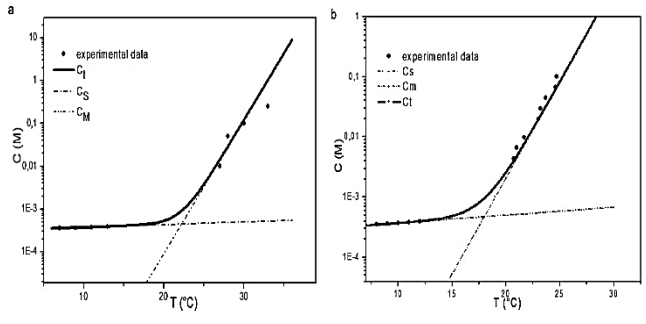

Fig. 9. Variation of the surfactant solubility with temperature (a) CTAB and (b) CPC.

This latter zone is in equilibrium along the solubility curve with a biphasic domain where a micellar solution is in equilibrium with the hydrated crystal solid phase (zone III). The fourth zone (IV) is constituted by a biphasic system where molecular solution is in equilibrium with hydrated crystal (saturated solution). This compartmentalization is only compatible with the mass action model as already shown in other surfactant systems.

For CTAB surfactant, at T_k point, monomeric surfactant solution is in equilibrium with both micellar and hydrated crystal phases. However, for CPC surfactant, since an unstable phase can emerge following the incubation time effect, several T_k points may be defined and a new fifth zone can be drawn.

This CTAB phase diagram is similar to the diagram of Matsuki *et al* [38] who used the differential scanning calorimetry to deduce these phase domains. While for CPC surfactant, Satake *et al.* [39] showed a phase diagram similar to our diagram deduced from a different characterization technique.

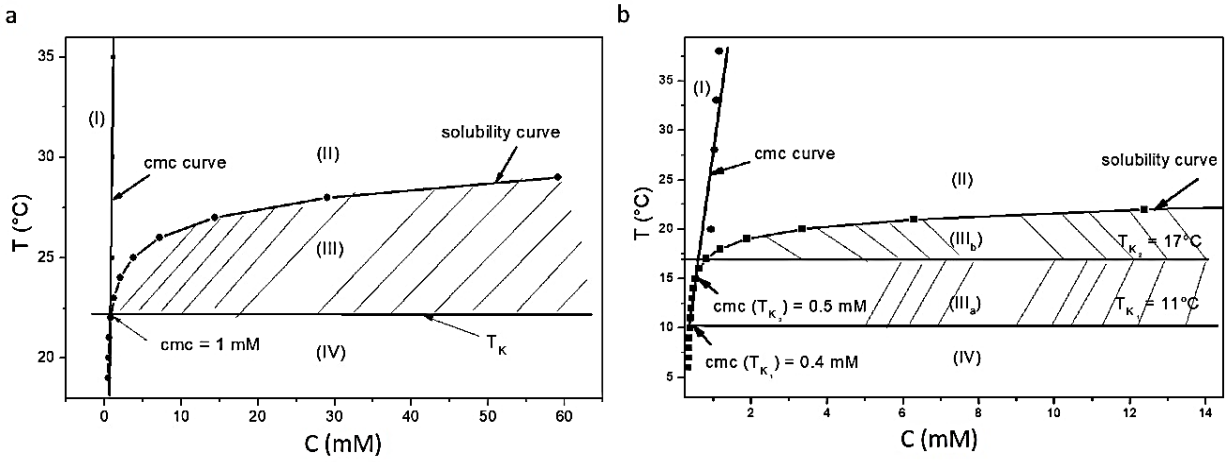

Fig. 10. Partial phase diagram of the (a) CTAB and (b) CPC surfactants in water.

Table 4. Thermodynamic parameters at different temperatures of CTAB and CPC

CTAB			
Temperature (°C)	$\Delta G°_m$ (KJ.mol^{-1})	$\Delta H°_m$ (KJ.mol^{-1})	$\Delta S°_m$ (J.mol^{-1}.K^{-1})
25	-48.89	-27.89	70.8
30	-48.97	-28.51	67.5
35	-49	-28.97	65
CPC			
Temperature (°C)	$\Delta G°_m$ (KJ.mol^{-1})	$\Delta H°_m$ (KJ.mol^{-1})	$\Delta S°_m$ (J.mol^{-1}.K^{-1})
28	-44.634	-32.283	41
33	-44.835	-32.801	39
35	-44.913	-33.011	38
38	-45.027	-33.327	37

Thus, from solubility parameters, it is possible to determine the aggregation number of the micelles, *n*, using the equation proposed by Moroi *et al.* [37] which states that the solubility above T_k depends on the average micelle aggregation number according to the following equation:

$$C_2(T) = C_2(T_K)[\frac{C_1(T)}{C_1(T_k)}]^n \quad (9)$$

Eq. (9) applied to sodium dodecyl sulfate (SDS) and HFDPyI micelles lead to n = 66 at 289 K [5] and n = 20 at 333 K [7] respectively and gives n = 27 at 280.7 K for tetracaine surfactant [6]. Once applied to the two studied surfactants one finds n = 25 for CPC and n = 53 for CTAB. From these results, it is possible to determine some micellization thermodynamic parameters according to the mass action model and assuming Phillips' definition [40] of the *cmc* for an ionic surfactant.

The standard Gibbs free energy change per mole of surfactant ion is given by:

$$\Delta G^o_{mic} = (1 + m/n)\, RT \ln X_{cmc} + (RT/n) \ln [2n\,(m + n)] \quad (10)$$

where m is the average number of counter-ions attached to the micelle, and X_{cmc} is the mole fraction at *cmc* [41]. The values of ΔG^o_{mic} obtained at different temperatures enable to determine the standard enthalpy of aggregation ΔH^o_{mic}, by applying the Gibbs-Helmholtz equation and further deduce the standard entropy of aggregation ΔS^o_{mic} from equations:

$$\Delta H^o_{mic} = \left(\frac{\partial \Delta G^o_{mic} / T}{\partial (1/T)} \right)_P \quad (11)$$

and

$$\Delta G^o_{mic} = \Delta H^o_{mic} - T\Delta S^o_{mic} \quad (12)$$

The obtained thermodynamic parameters values are shown on table 4. With these thermodynamic parameters in hand, one can show the dependence with temperature of the three energetic properties as illustrated in figure 11. Both enthalpy and entropy contribute favorably to the aggregation of the CTAB and CPC surfactants.

It is interesting to note that while enthalpy contribution increases with temperature entropy of aggregation decreases. Thus, the aggregation of the surfactant becomes slightly more exothermic with an increase in temperature (negative ΔH^o_{mic} values), suggesting that the London-dispersion forces are the major contributor. The contribution of the entropy term increases at low temperatures, a feature ascribed to the well-established hydrophobic effect [42], but without overcoming the enthalpy one which stands as the major contributor to the ΔG^o_{mic} values These behaviors lead us to draw the enthalpy–entropy compensation plot in figure 12.

The influence of water molecules and associated hydration/dehydration processes on the creation of surfactant micelles in an aqueous solution is responsible for the ΔH°/ΔS° compensatory effect which is ruled by the following equation [43].

$$\Delta H^\circ_m = \Delta H^{\circ,*}_m + T_c\, \Delta S^\circ_m \quad (13)$$

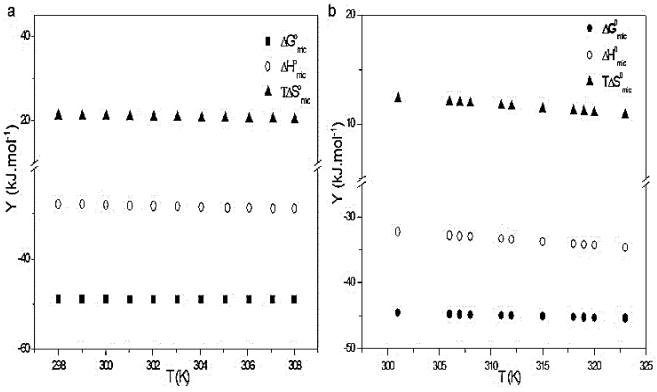

Fig. 11. Standard Gibbs energy, ΔG^o_{mic}; standard enthalpy, ΔH^o_{mic}; and standard entropy $T\Delta S^o_{mic}$, for the micellization process of the (a) CTAB and (b) CPC surfactant in water.

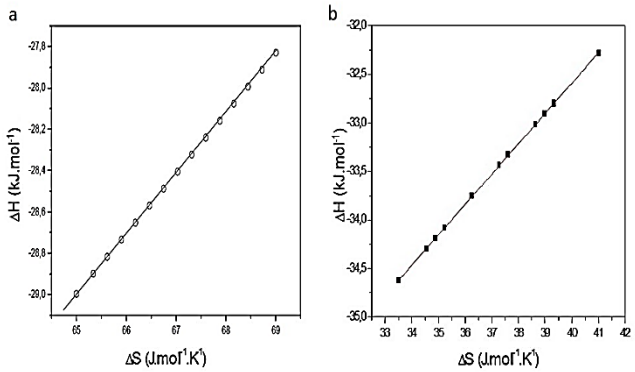

Fig. 12. Variation of ΔH^o_{mic} vs ΔS^o_{mic} for the (a) CTAB and (b) CPC surfactants in water showing the enthalpy-entropy compensation effect.

where the slope of this representation is known as the compensation temperature (T_c). As indicated by the linear behavior, the compensation effect is evident in figure 12, with a compensation temperature of T_c = 291 ± 2.5 K for CTAB close to the literature reported values (T_c = 276.89 [44] 287.91 [45] . For CPC surfactant, T_c = 312 K is deduced, a high value compared to one observed by Sultana *et al.*[46] T_c = 291.86K.

5. Conclusion

The purpose of this study was to investigate the thermodynamics of the micellization process of two surfactants (CTAB and CPC) by different techniques such as tensiometry, dynamic light scattering, and conductivity. From the analysis of conductivity, parameters such as the *cmc*, T_k , average micelle aggregation number, *n*, and the change of solubility with temperature were determined, and partial phase diagrams were drawn. Tensiometry has confirmed the surface activity of the two surfactants as well as their purity and has enabled the determination of the *cmc* values for each surfactant (*cmc* = 0.85 mM for CPC and *cmc* = 1 mM for CTAB). From DLS measurements it was demonstrated that the incubation time of solutions before experiments influences the phase diagram of the CPC system. When the incubation time is less than 24 h different micellar species coexist, the metastable ones disappear with temperature increase and only one micellar specie is resolved beyond a specific temperature. For CTAB surfactant, the incubation time effect is not detected and the system exhibits only one Krafft temperature at 24°C and one kind of micellar species. the conductivity analysis showed also that the CPC system exhibit complex curves compared to ones obtained with CTAB and different Krafft temperatures can be identified for a given incubation time as confirmed by DLS.

Both solubility and *cmc* curves were established for every system and the phase diagrams were drawn in light of the obtained values. The extraction of the aggregation number for every system enables to calculate the different thermodynamic parameters. The analysis of the variation of the free energy ΔG^o_{mic}, standard enthalpy of aggregation ΔH^o_{mic}, and the standard entropy of aggregation ΔS^o_{mic} shows that the aggregation process is enthalpy-driven. The entropy-enthalpy compensation temperatures are 291 K for CTAB and 312 K for CPC. The overall investigation underlines the utility of the combination of different techniques to explore these systems especially the conductometry and DLS which confirm their abilities to investigate special surfactants such as CPC which merits more extended attention.

Acknowledgement

The authors thank the DGRSDT and Mascara University, Algeria for technical support.

References

[1] J. Bergfreund, S. Siegenthaler, V. Lutz-bueno, P. Bertsch, P. Fischer, Surfactant Adsorption to Different Fluid Interfaces. *Langmuir.*, 37 (2021) 6722−6727.

[2] R.A. Gonçalves, K. Holmberg, B. Lindman, Cationic surfactants: A review, J. Mol. Liq., 375(2023) 121335

[3] D. R. Perinelli, M. Cespi, N. Lorusso, G. F. Palmieri, G. Bonacucina, P. Blasi, Surfactant Self-Assembling and Critical Micelle Concentration: One Approach Fits All, Langmuir., 36 (2020) 5745–5753.

[4] A. Tauzin, E. R. Dionne, A. Badia, The aggregation and micellization of ionic surfactants in aqueous solution detected using surface-confined redox and ion-pairing reactions. Electrochim. Acta., 326 (2019) 134991.

[5] R. Gaboriaud, G. Charbit F. Dorion, Equilibre de dissolution – Micellisation. *J. Chim. Phys.*, 81 (1984) 497–504.

[6] C. Zelmat, T. Fergoug, M. Azayez, N. Meddah, F. Chater, H. Boudjoras, Y. Bouhadda, Micellar and solubility properties of drug tetracaine-hydrochloride from thermal conductivity measurements. *J. Mol. Liq.*, 293 (2019) 111572.

[7] T. Fergoug, D. Bendedouch, E. Aicart, Characterization of the 1-heptodecafluorodecyl-pyridinium iodide in solution: Partial phase diagram and micellar properties from conductivity and surface tension. Colloids Surf A Physicochem. Eng. Asp., 237 (2004) 95–103.

[8] A. A. Atia, M. M. Saleh, Inhibition of acid corrosion of steel using cetylpyridinium chloride. *J. Appl. Electrochem.*, 33 (2003) 171–177.

[9] V. Pandarinathan, K. Lepková, S. I. Bailey, R. Gubner, Evaluation of corrosion inhibition at sand-deposited carbon steel in CO_2-saturated brine. *Corros. Sci.*, 72 (2013) 108–117.

[10] J. ArockiaSelvi, P. Kamaraj, M. Arthanareeswari, T. PushpaMalini, S. Mohanapriya, N. Subasree, Effect of Cetylpyridinium chloride on corrosion inhibition of mild steel in chloride environment. *Mater. Today Proc*., 14 (2019) 264–270.

[11] M. Abdullahi, A. K. Usman, A. M. Sani, K. Danazumi, A. U. Umar, J. Yusuf, Investigation of some expired antibiotic drugs: Effect on the corrosion inhibition of mild steel in 0.1 M HCl medium via experimental and molecular dynamics simulation. Chem. Rev. Lett., 5 (2022) 217–225.

[12] T. M. Miranda, A.R. Oliveira, L.M.D. Andrade, G.F. Silva, J.G. da Silva, G.F. Ferreira, A.M.L. Denadai, Mechanisms of interaction of Cetylpyridinium chloride with Staphylococcus aureus in the presence of β -cyclodextrin. J. Incl. Phenom. Macrocycl. Chem., 97(2020) 205–215.

[13] X. Mao, D. Auer, W. Buchalla, K. Hiller, T. Maisch, Cetylpyridinium chloride: mechanism of action, antimicrobial efficacy in biofilms and potential risks of resistance. Antimicrob. Agents Chemother., 64 (2020) 10-1128.

[14] A. Rawlinson, S. Pollington, T.F. Walsh, D.J. Lamb, I. Marlow, J. Haywood, P. Wright, Efficacy of two alcohol-free cetylpyridinium chloride mouthwashes –randomized double-blind crossover study. J Clin Periodontol., 35 (2008) 230–235.

[15] P. Raut, S.R. Weller, B. Obeng, B.L. Soos, B.E. West,

C.M. Potts, S. Sangroula, M.S. Kinney, J.E. Burnell, B.L. King, J.A. Gosse, S.T. Hess, Cetylpyridinium chloride (CPC) reduces zebrafish mortality from influenza infection : Super-resolution microscopy reveals CPC interference with multiple protein interactions with phosphatidylinositol 4, 5-bisphosphate in immune function. Toxicol. Appl. Pharmacol., 440 (2022)115913.

[16] S. A. Siadati, M. A. Rezvanfar, E. Babanezhad, A. Beheshti, M. Payab, Harmony of operations of some vitamins in controlling the 2019-nCoV virus based on scientific reports. Chem. Rev. Lett., 3 (2020) 202–206.

[17] S. Majedi S. Majedi, Existing drugs as treatment options for COVID-19: A brief survey of some recent results. J. Chem. Lett., 1 (2020) 2–8.

[18] M. A. Bhat, A. A. Dar, A. Amin, P. I. Rashid, G. M. Rather, Temperature dependence of transport and equilibrium properties of alkylpyridinium surfactants in aqueous solutions. J. Chem. Thermodyn., 39 (2007) 1500–1507.

[19] S.Sasaki, Metastable crystalline lamella of cetylpyridinium chloride in the Krafft transition. J. Phys. Chem. B., 111 (2007) 2473–2476.

[20] S. Sasaki, Kinetic Studies on Hydrated Solid Transform of Cetylpyridinium Chloride in Aqueous Solution. J. Phys. Chem. B., 113 (2009) 8545–8551.

[21] L. Abezgauz, K. Kuperkar, P. A. Hassan, O. Ramon, P. Bahadur, D. Danino, Effect of Hofmeister anions on micellization and micellar growth of the surfactant cetylpyridinium chloride. J. Colloid Interface Sci., 342 (2010) 83–92.

[22] G. Ghosh , P. K. Bhattacharya, Hexavalent chromium ion removal through micellar enhanced ultrafiltration. Chem. Eng. J., 119 (2006) 45–53.

[23] S. K. Mehta, S. Chaudhary, K. K. Bhasin, Self-assembly of cetylpyridinium chloride in water – DMF binary mixtures: A spectroscopic and physicochemical approach. J. Colloid Interface Sci., 321 (2008) 426–433.

[24] N. Islam, K. Chandra, Effect of Electrolytes on the Krafft Temperature of Cetylpyridinium Chloride in Aqueous Solution. J Surfact Deterg., 17 (2014) 525–530.

[25] W. Müller, Extraction liquide-solide des cations métalliques par des cations amphiphiles, Ph.D thesis, Montpellier II University, Montpellier, France (2010).

[26] S. Sasaki, Transformation relationships among monomers, micelles, metastable solid, and stable solid in aqueous cetylpyridinium chloride solution. J. Phys. Chem. B., 114 (2010) 11039–11045

[27] J. Mata, D. Varade, P. Bahadur, Aggregation behavior of quaternary salt based cationic surfactants. Thermochim. Acta., 428 (2005) 147–155.

[28] D. Varade, T. Joshi, V. K. Aswal, P. S. Goyal, P. A. Hassan, P. Bahadur, Effect of salt on the micelles of cetyl pyridinium chloride. Colloids Surfaces A Physicochem. Eng. Asp., 259 (2005) 95–101.

[29] S. K. Shah , A. Bhattarai, Interfacial and Micellization Behavior of Cetyltrimethylammonium Bromide (CTAB) in Water and Methanol-Water Mixture at 298.15 to 323.15 K. J. Chem., 2020 (2020) 13.

[30] T. Mukhim ,K. Ismail, Micellization of cetylpyridinium chloride in aqueous lithium chloride, sodium chloride and potassium chloride media. J. Surf. Sci. Technol., 21 (2005) 113–127.

[31] T. Chakraborty, S. Ghosh, S. P. Moulik, Micellization and related behavior of binary and ternary surfactant mixtures in aqueous medium: Cetyl pyridinium chloride (CPC), Cetyl trimethyl ammonium bromide (CTAB), and polyoxyethylene (10) cetyl ether (Brij-56) derived system. J. Phys. Chem. B., 109 (2005) 14813–14823.

[32] Y. Mirgorod, A. Chekadanov, T. Dolenko, structure of micelles of sodium dodecyl sulphate in water: an x-ray and dynamic light scattering study. Chem. J. Mold.,14 (2019) 107–119.

[33] A. Kadiri, T. Fergoug, K. Sebakhy, Y. Bouhadda, R. Aribi, F. Yssaad, Z. Daikh, M. El Hariri El Nokab, P.H.M. Van Steenberge, Insights into the Characterization of the Self-Assembly of Different Types of Amphiphilic Molecules Using Dynamic Light Scattering. ACS Omega., 8 (2023) 47714–47722.

[34] J. Ž. Manojlović, The Krafft temperature of surfactant solutions. Therm. Sci., 16 (2013) 631–641.

[35] J. Ž. Manojlović, Hysteresis of conductivity in a micellar surfactant solution near the Krafft point. J. Serb. Chem. Soc., 85 (2020) 67–78.

[36] C. Vautier-Giongo B. L. Bales, Estimate of the ionization degree of ionic micelles based on Krafft temperature measurements. J. Phys. Chem. B., 107 (2003) 5398–5403.

[37] Y. Moroi, R. Sugil, R. Matuura, Examination of micelle formation by phase rule. J. Colloid Interface Sci., 98 (1984) 184–191.

[38] H. Matsuki, R. Ichikawa, S. Kaneshina, H. Kamaya, I. Ueda, Differential scanning calorimetric study on the Krafft phenomenon of local anesthetics. J. Colloid Interface Sci., 181(1996) 362–369.

[39] H. Satake, H. Matsuki, S. Kaneshina, Colloidal properties of aqueous local anesthetic tetracaine solutions. Colloids Surfaces A Physicochem. Eng. Asp., 71(1993)135–140.

[40] J. N. Phillips, The energetics of micelle formation. Trans. Faraday Soc., 51 (1955) 561–569.

[41] A. Chatterjee, S. P. Moulik, S. K. Sanyal, B. K. Mishra, P. M. Puri, Thermodynamics of micelle formation of ionic surfactants: A critical assessment for sodium dodecyl sulfate, cetyl pyridinium chloride and dioctyl sulfosuccinate (Na salt) by microcalorimetric, conductometric, and tensiometric measurements. J. Phys. Chem. B., 105 (2001) 12823–12831.

[42] D. F. Evans , H. Wennerström , The Colloidal Domain - where physics, chemistry, biology, and technology meet, Wiley-VCH, USA (1999).

[43] M. A. Hoque , F. Ahmed, M.A. Halim, M.R. Molla, S. Rana, M.A. Rahman, M.A. Rub, Influence of salt and temperature on the interaction of bovine serum albumin with cetylpyridinium chloride: Insights from experimental and molecular dynamics simulation. J. Mol. Liq., 260 (2018) 121-130.

[44] M. Alam , M. Robel, S. Rana, M. Abdul, N. Azum, A. Hoque, S.E. Kabir, Aggregation behavior of cetyltrimethylammonium bromide and tetradecyltrimethylammonium bromide in aqueous / urea solution at different temperatures : Experimental and theoretical investigation. J. Mol. Liq., 285 (2019) 766–777.

[45] M. A. Hoque, M.M. Alam, M.R, Molla , S. Rana, M.A. Rub, M.A. Halim, M.A. Khan, F. Akhtar, Interaction of cetyltrimethylammonium bromide with drug in aqueous/electrolyte solution: A combined conductometric and molecular dynamics method study. Chinese J. Chem. Eng., 26 (2018) 159–167.

[46] S. Sultana, M. D. H. Alam, M. A. H. Shumon, Physico-chemical study of the interaction between levofloxacin hemihydrate Drug with Cetylpyridinium chloride in aqueous medium: Conductometric and spectrophotometric investigation. Int J Chem Stud., 8 (2020) 15–26.